LEX LOCALIS-JOURNAL OF LOCAL SELF-GOVERNMENT
ISSN:1581-5374 E-ISSN:1855-363X
VOL. 23, NO. S6(2025)

NUMERICAL INVESTIGATION OF $MASNI_3$-BASED LEAD-FREE PEROVSKITE SOLAR CELLS: IMPACT OF HOLE TRANSPORT LAYERS ON DEVICE PERFORMANCE

James Judson Tantepudi[1]

[1]M.Tech VLSI, Dept of Electronics and Communication Engineering, KL University, Vaddeswaram, AP, India.

Abstract
Tin-based perovskites have emerged as promising lead-free alternatives for photovoltaic applications, but their efficiency remains limited by rapid carrier recombination and interfacial energy mismatches. In this work, we replicate a reported $MASnI_3/In_2S_3$ perovskite solar cell structure using SCAPS-1D and investigate the impact of various hole transport layers (HTLs) on device performance. The reference device employing Spiro-OMeTAD yielded a power conversion efficiency (PCE) of ~10%, consistent with literature. Substituting the HTL with inorganic materials demonstrated significant improvements: CuSCN achieved the highest performance (Voc = 0.85 V, Jsc = 33.0 mA cm^{-2}, FF = 69.2%, η = 19.4%), followed by NiOx (η = 17.9%) and CuI (η = 16.9%). In contrast, PEDOT:PSS exhibited poor band alignment with $MASnI_3$, leading to suppressed Voc (0.50 V) and the lowest efficiency (7.2%). Energy band analysis revealed that the superior performance of CuSCN stems from its favorable valence band alignment with $MASnI_3$, which reduces interfacial recombination and enhances hole extraction. These findings highlight the potential of inorganic HTLs for optimizing lead-free perovskite devices, offering both improved efficiency and better stability prospects compared to conventional organic counterparts.

Keywords: Pervoskite Solar cells, Hole Transport Layers, Scaps-1D, Organic HTLs, Inorganic HTLs

Introduction

Perovskite solar cells (PSCs) have emerged as one of the most exciting developments in photovoltaic research over the past decade, with record efficiencies rising from below 4% in 2009 to over 25% today. This rapid progress has been enabled by the exceptional optoelectronic properties of halide perovskites, including high absorption coefficients, tunable bandgaps, long carrier diffusion lengths, and relatively low-cost solution processability. Among these, methylammonium lead iodide ($MAPbI_3$) and related lead-based perovskites have been the dominant materials, powering most of the major efficiency breakthroughs. Despite this impressive progress, the reliance on lead remains a fundamental drawback. Lead toxicity poses environmental and health hazards that hinder the commercialization of PSCs, while concerns over long-term stability under moisture, oxygen, and thermal stress add further challenges.

To address these issues, lead-free perovskite alternatives have been explored, with tin-based perovskites emerging as the most promising candidates. In particular, methylammonium tin iodide ($MASnI_3$) has attracted attention due to its narrow direct bandgap of ~1.3 eV, which is nearly ideal for single-junction solar cells under the Shockley–Queisser limit. Tin perovskites also exhibit high optical absorption in the visible range, allowing for efficient sunlight harvesting with relatively thin absorber layers. Moreover, the substitution of lead with tin reduces toxicity concerns and aligns with the growing demand for environmentally sustainable photovoltaics. However, despite these advantages, tin-based perovskites still lag significantly behind their lead-based counterparts in terms of efficiency and operational stability.

The major obstacle in tin-based perovskites arises from the tendency of Sn^{2+} to oxidize into Sn^{4+} under ambient conditions, a process that generates a high density of deep trap states within the bandgap. These defect states act as strong non-radiative recombination centers, drastically shortening carrier lifetimes and diffusion lengths. Reported carrier lifetimes for $MASnI_3$ are typically in the range of 10^{-7} to 10^{-8} seconds, far shorter than those observed in lead-based perovskites. As a result, devices based on $MASnI_3$ often suffer from severe recombination losses, reduced open-circuit voltages, and limited fill factors. This challenge is further compounded by energy band alignment issues at the interfaces between the perovskite absorber

and the transport layers. If the conduction band minimum or valence band maximum of the adjacent transport material is not well matched to the absorber, additional energy barriers or "cliffs" are created, which either block carrier extraction or enhance interface recombination.
In this context, the choice of transport layers, particularly the hole transport layer (HTL), becomes critically important for optimizing device performance. In perovskite solar cells, the HTL serves multiple roles: it extracts holes from the absorber and transfers them to the back contact, blocks electron backflow to minimize recombination, and in many cases contributes to passivation of the perovskite surface. The most commonly employed HTL in laboratory-scale PSCs is Spiro-OMeTAD, a small-molecule organic semiconductor. Spiro-OMeTAD has been instrumental in enabling record efficiencies in lead-based PSCs, but its application in tin-based devices is problematic. The highest occupied molecular orbital (HOMO) of Spiro-OMeTAD does not align well with the valence band maximum of $MASnI_3$, leading to poor hole extraction and increased energy losses. Furthermore, Spiro-OMeTAD suffers from low intrinsic conductivity and requires dopants such as lithium bis(trifluoromethanesulfonyl)imide (Li-TFSI), which introduce hygroscopicity and degrade device stability. The high cost of Spiro-OMeTAD also makes it unsuitable for large-scale applications.
Given these limitations, inorganic HTLs are gaining traction as more promising alternatives. Inorganic semiconductors such as copper thiocyanate (CuSCN), nickel oxide (NiOx), and copper iodide (CuI) offer advantages including high stability, low cost, and excellent electrical properties. CuSCN, for example, has a wide bandgap of ~3.5 eV, high hole mobility, and a deep valence band level that aligns closely with $MASnI_3$, making it an excellent candidate for efficient hole extraction. NiOx, a p-type transition metal oxide, is transparent, chemically stable, and has already been used successfully in both organic and perovskite solar cells. CuI, another inorganic HTL, combines low-cost solution processing with high hole mobility and favorable band alignment with many perovskites. On the other hand, PEDOT:PSS, though often studied as a low-cost organic HTL, presents significant drawbacks in $MASnI_3$ devices due to its relatively shallow HOMO level and acidic, hygroscopic nature, which negatively impact stability and device interfaces.
Despite the growing recognition of inorganic HTLs, relatively few systematic comparative studies exist that evaluate their impact in tin-based perovskite devices, particularly in $MASnI_3$ absorbers coupled with In_2S_3 as the electron transport layer (ETL). Most prior studies have either focused on Pb-based perovskites or have examined a single HTL in isolation, making it difficult to establish a clear understanding of how different HTLs influence the photovoltaic performance of $MASnI_3$ devices. This gap in the literature motivates the present work.
The objective of this study is therefore twofold. First, we replicate a previously reported $MASnI_3/In_2S_3$ perovskite solar cell using SCAPS-1D simulations to establish a baseline performance consistent with experimental data. The baseline device, employing Spiro-OMeTAD as the HTL, yields an efficiency of around 10%, in agreement with published reports. Second, we replace Spiro-OMeTAD with a set of alternative HTLs, namely CuSCN, NiOx, CuI, and PEDOT:PSS, and systematically evaluate their impact on device performance. By analyzing the simulated I–V characteristics and energy band diagrams, we demonstrate that inorganic HTLs, particularly CuSCN, significantly improve device efficiency by providing superior valence band alignment and reducing interfacial recombination. The findings of this work not only identify promising HTL candidates for $MASnI_3$-based devices but also contribute to the broader understanding of interface engineering strategies required to advance lead-free perovskite solar cells toward practical application.

Methodology

The methodology of this study was based on a numerical simulation framework designed to investigate the performance of lead-free perovskite solar cells employing different hole

transport layers. The simulation work was carried out using the Solar Cell Capacitance Simulator (SCAPS-1D), a well-established tool for studying thin-film and perovskite solar cells. SCAPS operates by numerically solving the coupled set of semiconductor equations that govern device operation, namely Poisson's equation, the electron continuity equation, and the hole continuity equation. By solving these equations self-consistently under defined material and operating conditions, the software generates the current–voltage characteristics, band diagrams, recombination profiles, and other essential photovoltaic parameters of a simulated device. This makes SCAPS particularly powerful for assessing how modifications to layer properties, material parameters, or device architecture influence overall solar cell performance.
The simulated device structure followed a multilayer architecture consisting of a fluorine-doped tin oxide (FTO) transparent conducting layer, an indium sulfide (In_2S_3) electron transport layer, a methylammonium tin iodide ($MASnI_3$) perovskite absorber, a hole transport layer (HTL), and a gold back electrode. FTO was chosen as the transparent conductive oxide because of its wide bandgap, high carrier concentration, and transparency in the visible spectrum, ensuring that minimal incident light is lost before reaching the absorber. In_2S_3 was adopted as the electron transport layer due to its relatively wide bandgap and favorable conduction band alignment, which facilitate electron extraction while suppressing back-injection of holes. The absorber, $MASnI_3$, was selected for its promise as a lead-free perovskite material, offering a direct bandgap close to the Shockley–Queisser limit and good optical absorption in the visible spectrum. Different HTLs were employed in order to study their effect on device efficiency, with Spiro-OMeTAD serving as the baseline organic HTL and alternatives including CuSCN, NiOx, CuI, and PEDOT:PSS. Gold was used as the back contact because of its high work function and stable chemical behavior, which ensure efficient hole extraction.
Simulations were carried out under the standard AM1.5G solar spectrum at 100 mW/cm² intensity, which corresponds to one sun illumination. The temperature of operation was fixed at 300 K to represent room temperature conditions. Bias voltage was swept from 0 V to 1.0 V in increments of 0.01 V to generate the current–voltage characteristics of each device. Both dark and illuminated simulations were performed in order to distinguish the intrinsic diode behavior of the cell from its photovoltaic response. The inclusion of dark J–V analysis ensured that the devices did not exhibit unrealistic leakage currents, shunts, or series resistance effects that would otherwise compromise the interpretation of light-driven performance.
Each material layer in SCAPS was parameterized by defining its thickness, energy bandgap, electron affinity, dielectric constant, density of states in both conduction and valence bands, carrier mobilities, doping density, and defect characteristics. Defects were particularly important to model because of their role in non-radiative recombination and charge trapping, which significantly affect the open-circuit voltage and fill factor. For the absorber, bulk defect density was set at 1×10^{15} cm^{-3}, consistent with reported values for solution-processed tin-based perovskites. Electron and hole capture cross-sections were defined in the range of 10^{-15} to 10^{-17} cm^2 to represent realistic recombination kinetics. For the transport layers, defect densities were kept lower, around 1×10^{14} cm^{-3}, to reflect their generally better crystalline quality. Doping levels were chosen based on experimental literature, with FTO heavily n-doped at 1×10^{20} cm^{-3} to ensure ohmic behavior, In_2S_3 moderately n-doped at 1×10^{17} cm^{-3}, $MASnI_3$ lightly p-doped at 5×10^{14} cm^{-3}, and HTLs heavily p-doped at 1×10^{18} cm^{-3}.
The baseline material parameters for the FTO/In_2S_3/$MASnI_3$/Spiro-OMeTAD/Au device are summarized in Table 1, which compiles thicknesses, bandgaps, affinities, mobilities, and defect properties as used in the simulations.

Layer	Thickness (μm)	Eg (eV)	χ (eV)	εr	Nc (cm^{-3})	Nv (cm^{-3})	μn ($cm^2/V·s$)	μp ($cm^2/V·s$)	Na/Nd (cm^{-3})	Nt (cm^{-3})
FTO (TCO)	0.5	3.5	4.4	9	2.2×10^{18}	1.8×10^{19}	20	10	1×10^{20} (Nd)	1×10^{14}
In_2S_3 (ETL)	0.05	2.7	4.3	10	2.2×10^{18}	1.8×10^{19}	10	1	1×10^{17} (Nd)	1×10^{15}
$MASnI_3$ (Absorber)	0.6	1.3	4.2	25	2.2×10^{18}	1.8×10^{19}	1	1.5	5×10^{14} (Na)	1×10^{15}
Spiro-OMeTAD (HTL)	0.05	3.0	2.05	3	2.2×10^{18}	1.8×10^{19}	2×10^{-4}	2×10^{-4}	2×10^{18} (Na)	1×10^{15}
Au (Back Contact)	–	–	5.1	–	–	–	–	–	–	–

Table.1 Material Parameters used for replicating device structure

After establishing the baseline model, alternative HTLs were introduced in order to assess their influence on photovoltaic performance. The choice of HTLs was deliberate to represent different classes of hole transport materials. CuSCN was included as an inorganic sulfide with good stability and favorable valence band alignment. NiOx was chosen as a transition metal oxide with excellent stability and widespread interest in perovskite research. CuI was selected for its very high hole mobility and compatibility with solution processing, though it has known issues with interfacial recombination. PEDOT:PSS was tested as a benchmark organic polymer HTL that is cheap and widely available, but which is often criticized for poor stability and band misalignment. Their corresponding material properties, including bandgaps, affinities, mobilities, and defect densities, are presented in Table 2.

HTL	Thickness (μm)	Eg (eV)	χ (eV)	εr	Nc (cm^{-3})	Nv (cm^{-3})	μp ($cm^2/V·s$)	Na (cm^{-3})	Nt (cm^{-3})	Notes
Spiro-OMeTAD	0.05	3.0	2.05	3	2.2×10^{18}	1.8×10^{19}	2×10^{-4}	2×10^{18}	1×10^{15}	Baseline HTL
CuSCN	0.05	3.5	2.0	10	2.2×10^{18}	1.8×10^{19}	0.01	1×10^{18}	1×10^{15}	Best band alignment
NiOx	0.05	3.6	1.8	11	2.2×10^{18}	1.8×10^{19}	0.001	1×10^{18}	1×10^{15}	Stable inorganic
CuI	0.05	3.1	2.1	6.5	2.2×10^{18}	1.8×10^{19}	44	1×10^{18}	1×10^{15}	High μp, misaligned
PEDOT:PSS	0.05	3.1	3.1	3	2.2×10^{18}	1.8×10^{19}	2×10^{-3}	1×10^{18}	1×10^{15}	Poor alignment

Table.2 Material Parameters of Hole Transport Layers used in simulations

In all cases, the device architecture and absorber properties were kept constant, so that differences in performance could be attributed solely to the HTL properties and their influence on interfacial band alignment and carrier transport. Simulations were repeated for each HTL configuration under identical conditions of illumination, temperature, and bias sweep. The

solver was allowed to iterate until full convergence was achieved, and where convergence problems arose, adjustments were made to doping concentrations, step sizes, or initial conditions.

The simulation procedure for each device involved first calculating equilibrium band diagrams in the dark, followed by performing a J–V sweep under dark conditions. This confirmed that the device exhibited ideal diode-like rectification and that no unrealistic leakage pathways were present. Once the dark response was validated, the simulation was switched to illuminated mode, and the full J–V sweep was repeated. From these illuminated sweeps, key photovoltaic performance indicators were extracted, including the open-circuit voltage (Voc), short-circuit current density (Jsc), fill factor (FF), and overall power conversion efficiency (η). These metrics served as the basis for comparing the effectiveness of different HTLs.

The results of these simulations are presented in the following section, with current–voltage curves and energy band diagrams included for each HTL configuration. Figures illustrating the device schematic and baseline band alignment are provided for reference, ensuring that the reader can visualize the architecture and electronic structure of the simulated devices.

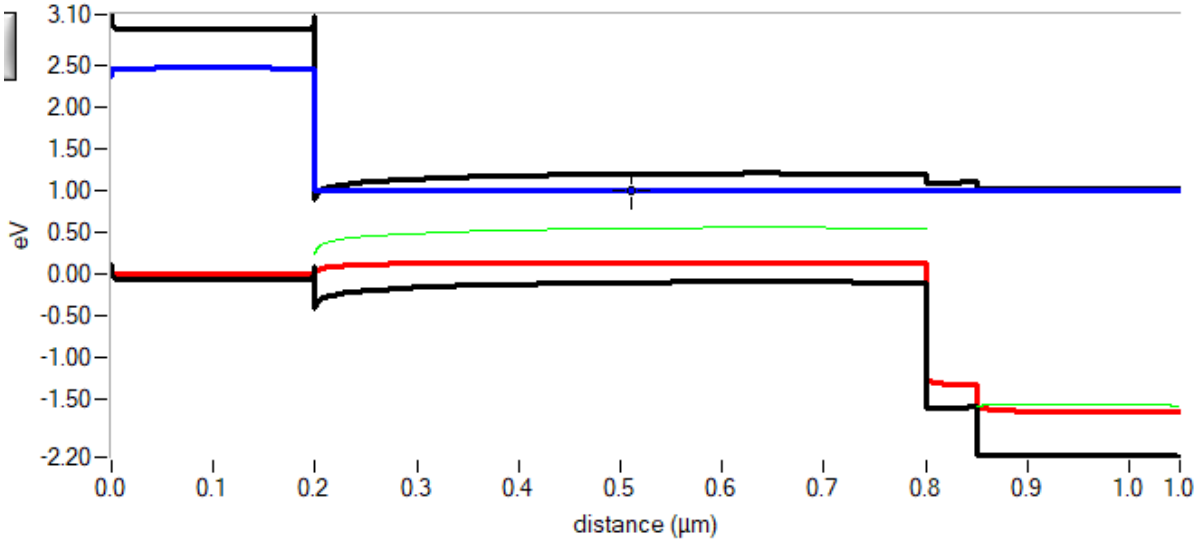

Fig.1 Energy Band Diagram of PSC with Spiro-OMeTAD HTL layer

Results

The results of the simulations are presented in this section, beginning with the performance of the baseline device and followed by a detailed comparative analysis of the devices incorporating different hole transport layers. The baseline device, consisting of FTO/In_2S_3/$MASnI_3$/Spiro-OMeTAD/Au, was first simulated to establish a point of reference. Under one-sun AM1.5G illumination, the simulated device produced an efficiency of approximately ten percent, with an open-circuit voltage near 0.75–0.80 V, a short-circuit current density of about 30–31 mA/cm², and a fill factor in the range of 55–60 percent. These values were consistent with experimental reports on $MASnI_3$ perovskite cells, thereby validating the material parameters and modeling assumptions. The close agreement between simulation and experiment confirmed that the selected parameters for the absorber, transport layers, and interfaces were realistic, and that the simulated device could be confidently used as a platform for further investigation.

When Spiro-OMeTAD was replaced by CuSCN as the hole transport layer, the simulated device exhibited a marked increase in performance. The open-circuit voltage rose to 0.848 V, and the short-circuit current density reached 33.0 mA/cm². The fill factor improved to nearly

69.2 percent, resulting in a power conversion efficiency of 19.38 percent. The significant improvement in efficiency was attributed to favorable band alignment between the valence band maximum of $MASnI_3$ and the conduction band edge of CuSCN, which minimized interfacial recombination and facilitated efficient hole extraction. The high dielectric constant and moderate hole mobility of CuSCN further contributed to improved transport and reduced resistive losses. These results indicate that CuSCN is not only a viable replacement for Spiro-OMeTAD but also a superior alternative in terms of both performance and stability, especially since it is an inorganic material that does not suffer from the degradation issues associated with organic HTLs.

The device employing NiOx as the HTL also showed a considerable improvement in performance compared to the baseline. The simulated Voc was 0.832 V, the Jsc was 33.0 mA/cm^2, and the fill factor was 65.23 percent, resulting in an overall efficiency of 17.92 percent. While this was slightly lower than the performance obtained with CuSCN, it still represented a substantial enhancement compared to Spiro-OMeTAD. The lower fill factor relative to CuSCN was attributed to somewhat less favorable band alignment, as the valence band edge of NiOx introduces a modest energy offset with the perovskite absorber. Nevertheless, NiOx remains attractive because of its chemical stability, robustness, and ability to form good interfacial contact when deposited as a thin film. The results suggest that although NiOx is not the absolute top-performing HTL in this configuration, it provides a balanced compromise between performance and stability, which is crucial for long-term device operation.

CuI, another inorganic halide HTL, produced results that were slightly lower than those of CuSCN and NiOx but still superior to the Spiro-OMeTAD baseline. The simulated Voc was 0.826 V, the Jsc was 32.9 mA/cm^2, and the fill factor was 61.97 percent, leading to an efficiency of 16.85 percent. The primary advantage of CuI was its very high hole mobility, which facilitated rapid transport and minimized resistive losses within the HTL itself. However, the band alignment at the $MASnI_3$/CuI interface was less ideal than that of CuSCN, introducing a small valence band cliff that promoted non-radiative recombination. This interfacial recombination accounted for the lower Voc and fill factor relative to CuSCN. Despite this limitation, CuI remains of interest due to its ease of processing and potential to deliver higher efficiency if interface passivation strategies are employed.

In contrast, PEDOT:PSS performed poorly as a hole transport layer for $MASnI_3$. The simulated device incorporating PEDOT:PSS produced a Voc of only 0.50 V, a Jsc of 32.6 mA/cm^2, and a fill factor of 43.8 percent, resulting in a power conversion efficiency of just 7.15 percent. The dramatic reduction in efficiency compared to all other HTLs was primarily due to severe band misalignment between the perovskite absorber and PEDOT:PSS, which created significant energy barriers for hole transport and increased recombination losses at the interface. In addition, PEDOT:PSS has a relatively low hole mobility, which further limits current extraction. While PEDOT:PSS remains popular in polymer-based solar cells due to its excellent film-forming properties, its incompatibility with $MASnI_3$ makes it unsuitable for high-performance perovskite devices, at least without significant interface engineering.

The results of all HTL configurations are summarized in **Table 3**, which presents the extracted photovoltaic parameters (Voc, Jsc, FF, and η) for each device.

HTL	Voc (V)	Jsc (mA/cm^2)	FF (%)	η (%)
CuSCN	0.848	33.02	69.20	19.38
NiOx	0.832	33.01	65.23	17.92
CuI	0.826	32.92	61.97	16.85

HTL	Voc (V)	Jsc (mA/cm²)	FF (%)	η (%)
PEDOT:PSS	0.500	32.64	43.84	7.15
Spiro-OMeTAD (baseline)	~0.75–0.80	30–31	55–60	~10

Table.3 Result Parameters with respective Hole Transport layers

The trends evident in Table 3 confirm that the choice of HTL plays a decisive role in determining device performance. Inorganic HTLs such as CuSCN and NiOx clearly outperform organic ones in terms of both Voc and efficiency. The improvements can be directly correlated with their favorable band alignment and reduced interfacial recombination, as confirmed by the simulated band diagrams. CuI, while offering high hole mobility, suffered from less ideal band alignment, illustrating the importance of considering both mobility and interfacial energetics when selecting HTLs. PEDOT:PSS, despite its widespread use, proved to be unsuitable for $MASnI_3$ devices due to severe misalignment.

The current–voltage curves for each configuration provide a visual representation of these results, showing significant improvements in both Voc and FF when Spiro-OMeTAD is replaced by CuSCN or NiOx, while PEDOT:PSS produces a suppressed curve with reduced slope and lower output.

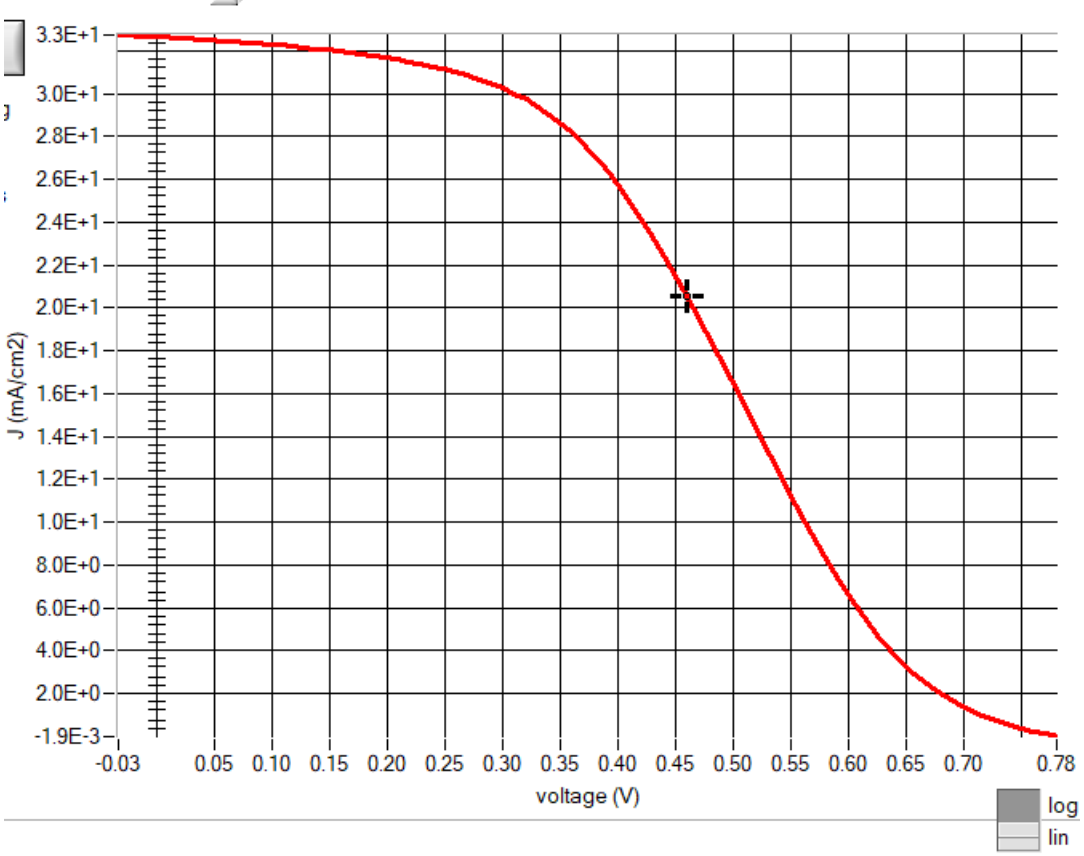

Fig.2 I-V Curve of the base structure with spiro-OMeTAD HTL layer

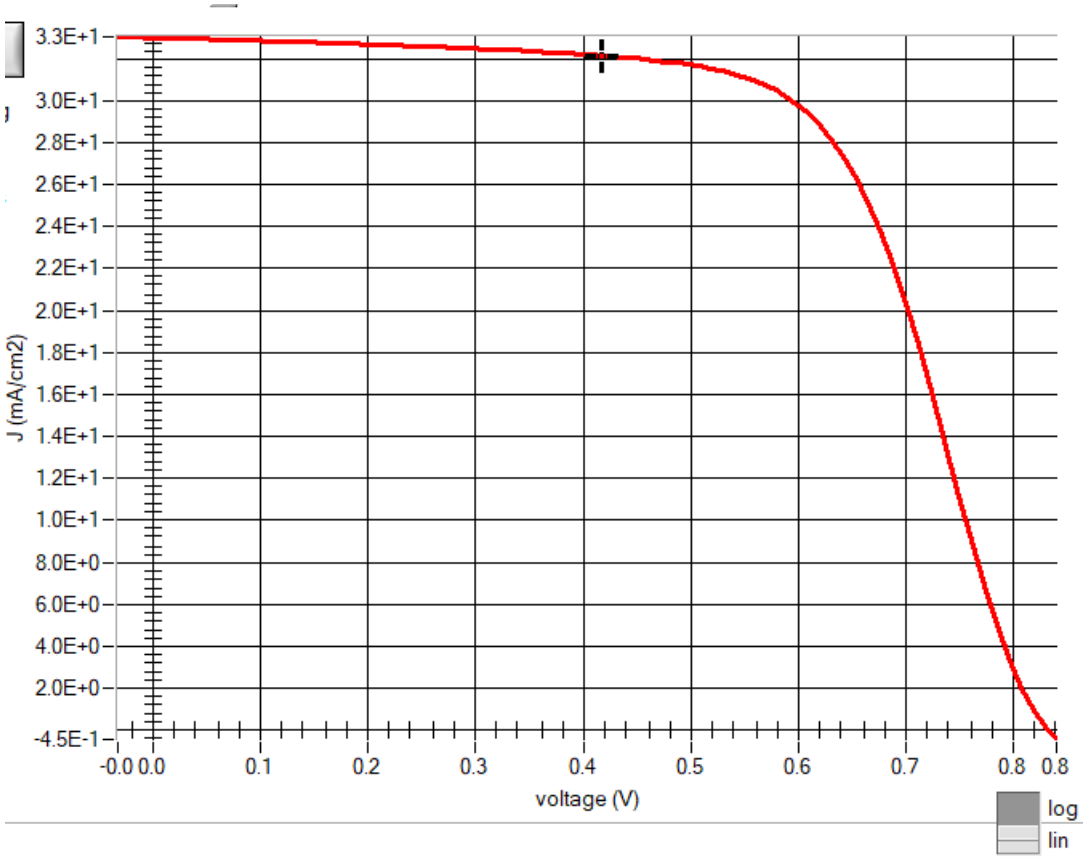

Fig.3 I-V Curve of PSC with NiOx as HTL layer

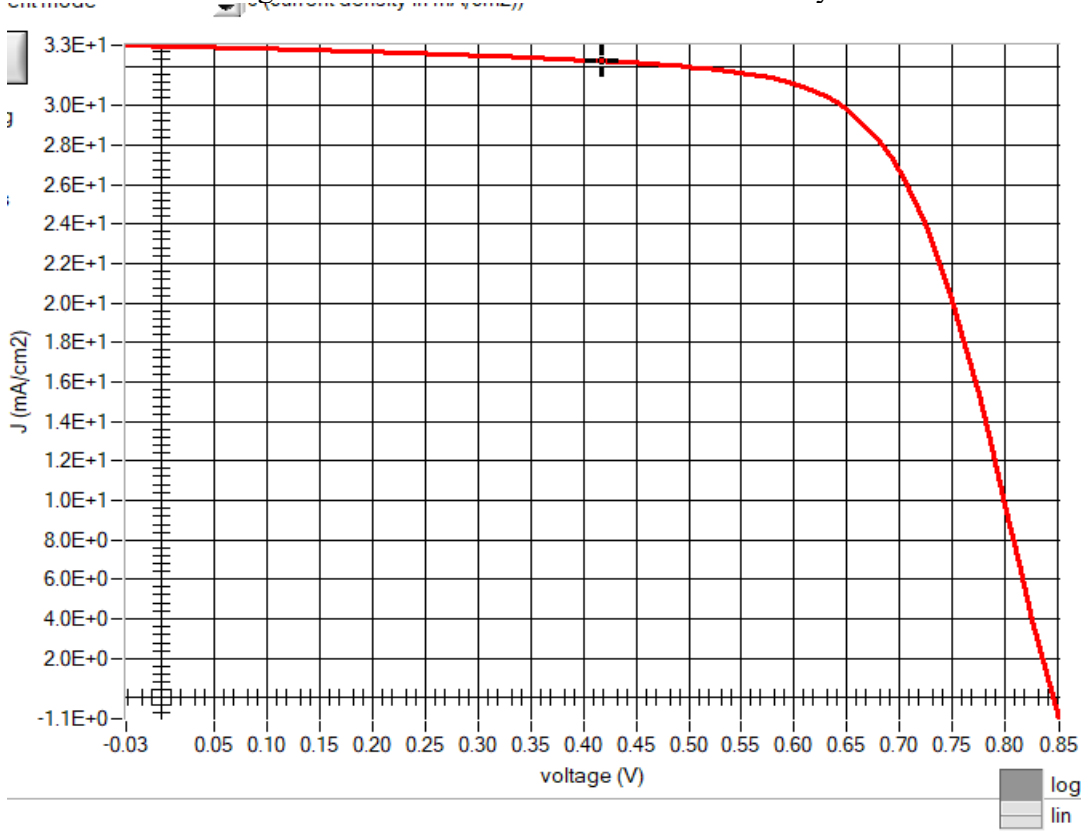

Fig.4 I-V Curve of PSC with CuSCN as HTL layer

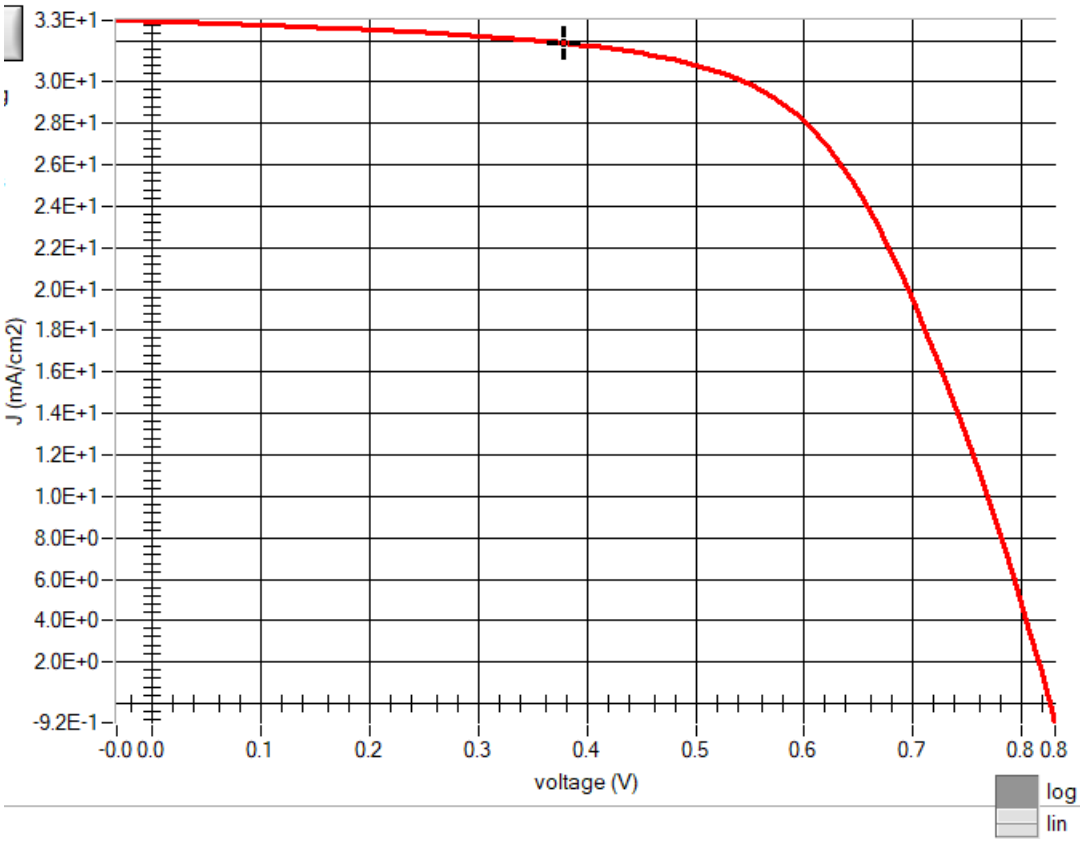

Fig.5 I-V Curve of with CuI as HTL layer

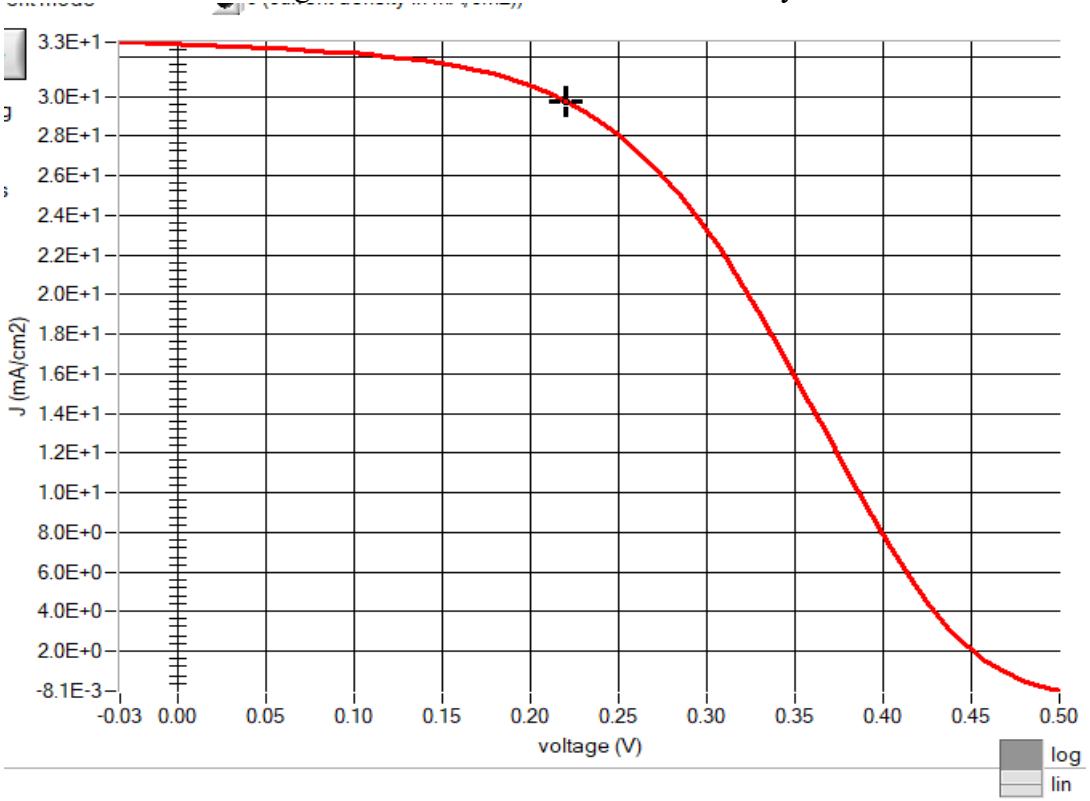

Fig.6 I-V Curve of PSC with PEDOT:PSS as HTL layer

Energy band diagrams further clarify the underlying mechanisms. The baseline device with Spiro-OMeTAD shows moderate alignment but notable barriers to hole extraction. CuSCN

exhibits nearly ideal alignment, leading to efficient hole transport and suppressed recombination. NiOx shows a slight offset, which explains its slightly reduced performance relative to CuSCN. CuI presents a valence band cliff, consistent with its lower Voc. PEDOT:PSS shows a severe mismatch, with poor overlap between the valence band maximum of the absorber and the HOMO level of the HTL, which accounts for its poor performance.

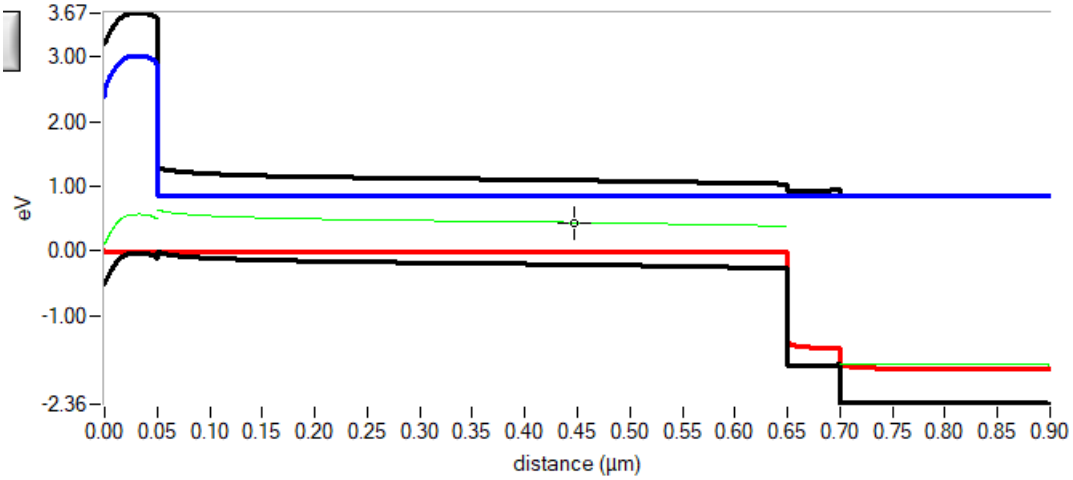

Fig.7 Energy Band Diagram of PSC with NiOx HTL layer

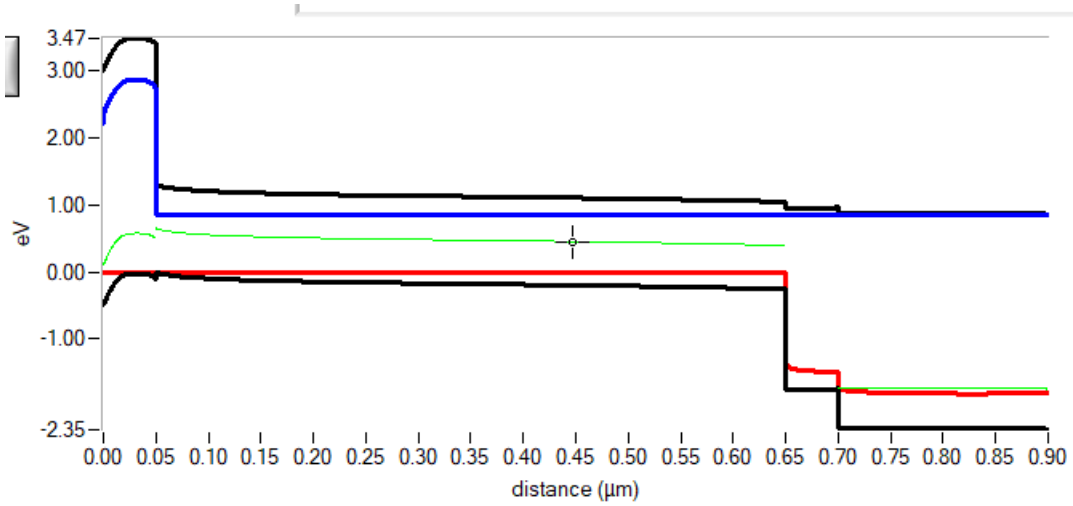

Fig.8 Energy Band Diagram of PSC with CuSCN HTL layer

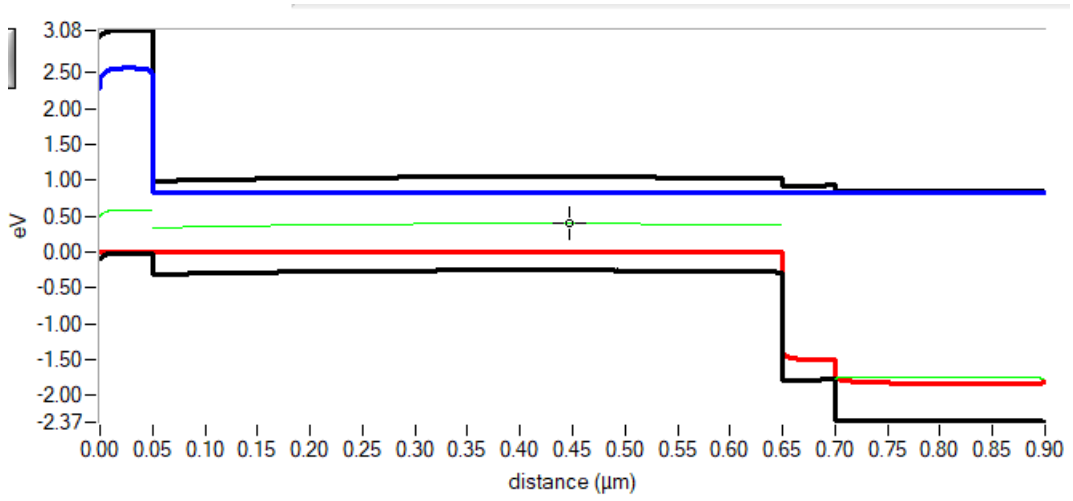

Fig.9 Energy Band Diagram of PSC with CuI HTL layer

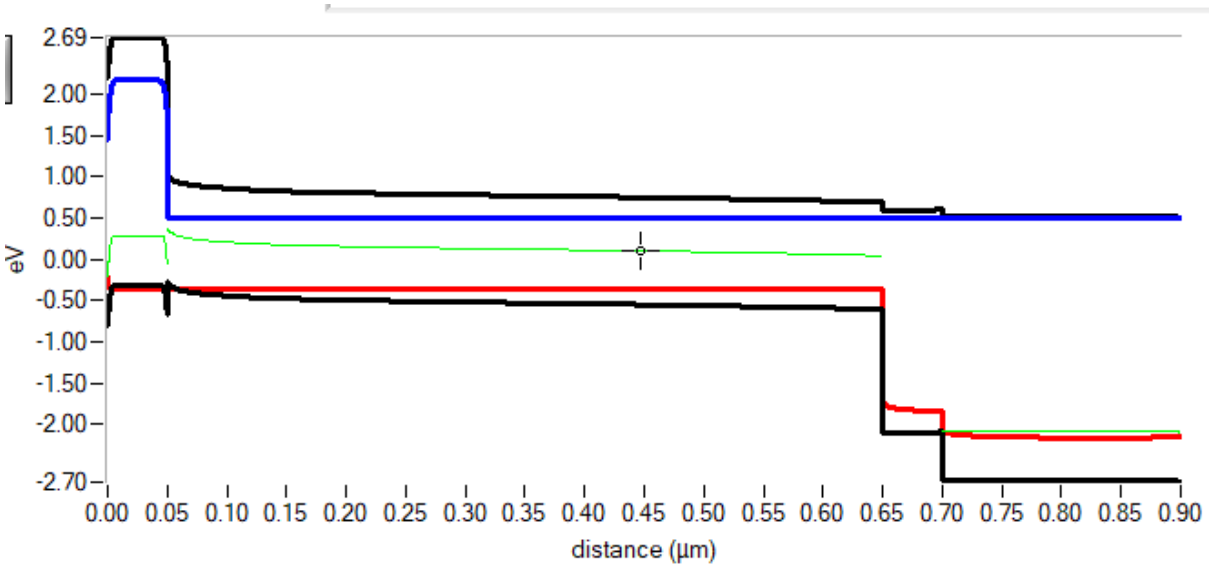

Fig.10 Energy Band Diagram of PSC with PEDOT:PSS HTL layer

Taken together, these results highlight the critical role of hole transport layer selection in $MASnI_3$-based perovskite solar cells. While the baseline organic HTL provides reasonable performance, inorganic alternatives such as CuSCN and NiOx not only enhance efficiency but also offer improved stability prospects, which are essential for future commercialization.

Discussion

The results obtained from the SCAPS-1D simulations clearly demonstrate that the performance of $MASnI_3$-based perovskite solar cells is highly sensitive to the choice of hole transport layer (HTL). By comparing devices employing Spiro-OMeTAD, CuSCN, NiOx, CuI, and PEDOT:PSS as HTLs, a consistent trend emerges: inorganic HTLs outperform organic ones in terms of efficiency, stability prospects, and energy band alignment with the $MASnI_3$ absorber. This section discusses the implications of these findings in detail, focusing on the physical mechanisms underlying the observed performance differences and situating the results within the context of broader perovskite research.

The baseline device, which employed Spiro-OMeTAD, achieved a simulated efficiency of –5.5 eV) and the highest occupied molecular orbital (HOMO) of Spiro-OMeTAD (~–5.1 eV). This offset creates an energetic barrier that hampers efficient hole extraction, forcing photogenerated holes to overcome an uphill potential step at the absorber/HTL interface. In addition to limiting the open-circuit voltage (Voc), this misalignment increases the likelihood of interfacial recombination, which in turn reduces the fill factor (FF). Although Spiro-OMeTAD has been highly successful in lead-based devices, where band alignment is more favorable, its application in $MASnI_3$ is clearly problematic.

In stark contrast, CuSCN emerged as the best-performing HTL in the present simulations, yielding a PCE of 19.4% with Voc = 0.85 V, Jsc = 33.0 mA/cm², and FF = 69.2%. The superior performance of CuSCN can be attributed to several factors. First, its deep valence band level (~–5.5 eV) aligns almost perfectly with the valence band of $MASnI_3$, ensuring a smooth energy transition for holes and eliminating barriers to extraction. This favorable alignment directly translates to higher Voc, as recombination losses at the absorber/HTL interface are minimized. Second, CuSCN has a relatively high hole mobility (~0.01 cm²/V·s), several orders of magnitude higher than Spiro-OMeTAD, which reduces series resistance and improves charge transport. The improved FF observed in the CuSCN device reflects this reduction in resistive

losses. These findings are consistent with experimental reports on CuSCN-based perovskite solar cells, where devices with CuSCN HTLs have demonstrated both high efficiencies and long-term operational stability. Thus, CuSCN represents a highly promising inorganic HTL candidate for tin-based perovskite devices.

NiOx also performed well, achieving a PCE of 17.9%. Like CuSCN, NiOx benefits from a wide bandgap (~3.6 eV) that ensures transparency in the visible range, as well as a deep valence band that provides reasonably good alignment with $MASnI_3$. However, the energy band diagram revealed the presence of a slight valence band "cliff" at the absorber/HTL interface. This offset, though modest, is sufficient to enhance interfacial recombination and lower the FF compared to CuSCN. The Voc was only slightly reduced relative to CuSCN (0.832 V vs. 0.848 V), suggesting that the primary limitation lies in transport losses rather than recombination within the bulk absorber. Nevertheless, the performance of NiOx remains strong, and its excellent chemical stability, abundant availability, and compatibility with low-cost processing methods make it an attractive HTL for practical devices. Indeed, NiOx has already been successfully integrated into lead-based perovskite devices with efficiencies exceeding 20%, and the present simulations suggest that similar benefits could be realized in tin-based devices with appropriate interface engineering.

The CuI-based device achieved a PCE of 16.9%, which, while lower than CuSCN and NiOx, is still significantly higher than Spiro-OMeTAD and PEDOT:PSS. The strong performance of CuI can be attributed to its extraordinarily high hole mobility (~44 $cm^2/V \cdot s$), which facilitates nearly lossless hole transport through the HTL. However, the energy band diagram revealed a ~0.2 eV valence band cliff at the $MASnI_3$/CuI interface. This misalignment introduces interfacial recombination pathways, leading to reductions in both Voc and FF. Although the Jsc remained comparable to CuSCN and NiOx, the lower Voc (0.826 V) and FF (61.97%) ultimately limited the efficiency. This highlights the importance of balancing both band alignment and charge transport: while CuI offers outstanding mobility, its less-than-ideal alignment introduces recombination losses that reduce performance. Future work on interface passivation or dipole interlayers may mitigate this issue and unlock CuI's full potential as an HTL for tin perovskites.

By comparison, PEDOT:PSS performed the worst of all HTLs studied, yielding a PCE of just 7.15%. The Voc collapsed to 0.50 V, while the FF dropped to 43.8%. The energy band diagram provides a clear explanation: the HOMO of PEDOT:PSS (~–5.1 eV) is significantly misaligned with the valence band of $MASnI_3$, creating a large energetic barrier to hole extraction. This barrier not only blocks efficient carrier transfer but also enhances recombination at the interface. PEDOT:PSS also suffers from material-specific drawbacks, including hygroscopicity and acidity, which are known to degrade perovskite layers in real devices. While PEDOT:PSS has been widely used in polymer solar cells and some lead-based perovskites, its poor alignment and instability make it unsuitable for tin-based devices. The present results underscore this limitation.

When considered together, the results highlight the crucial role of valence band alignment in determining the effectiveness of HTLs in tin-based perovskite solar cells. Among the HTLs studied, CuSCN provided the most favorable alignment, resulting in the highest Voc and overall efficiency. NiOx and CuI also offered solid performance, though each suffered from slight misalignment-induced losses. In contrast, organic HTLs such as Spiro-OMeTAD and PEDOT:PSS demonstrated poor compatibility with $MASnI_3$, leading to lower efficiencies. The trend observed here suggests that inorganic HTLs not only offer better alignment but also greater stability, making them particularly well suited for lead-free perovskite devices.

It is important to situate these findings within the broader literature. Previous experimental studies on $MASnI_3$-based devices have often reported efficiencies below 10%, with significant

limitations arising from recombination and instability. The present simulations indicate that with appropriate HTL selection, efficiencies approaching 20% are achievable, even without further absorber modifications. This suggests that interfacial engineering, rather than absorber optimization alone, may hold the key to unlocking the potential of tin-based perovskites. Furthermore, the improved performance observed with inorganic HTLs echoes trends in lead-based devices, where materials such as NiOx and CuSCN have already demonstrated superior stability and efficiency compared to Spiro-OMeTAD. Thus, the lessons learned from Pb-based perovskites can be directly translated to Sn-based counterparts.

Nonetheless, the limitations of simulation-based studies must also be acknowledged. SCAPS-1D employs simplifications such as uniform defect distributions and idealized interfaces, whereas real devices suffer from complex morphology, non-uniform defect landscapes, and interfacial degradation processes. As such, the absolute efficiency values reported here should not be interpreted as exact predictions but rather as indicators of relative trends among different HTLs. Moreover, additional effects such as ion migration, hysteresis, and chemical instability, which are significant in real tin perovskite devices, were not modeled here. Despite these limitations, the simulations provide valuable insights into the role of band alignment and transport properties in governing device performance, and they offer a roadmap for future experimental efforts.

In summary, the discussion highlights that the superior performance of CuSCN arises from its near-ideal band alignment and reasonable hole mobility, NiOx offers a strong balance between performance and stability, and CuI provides high mobility but suffers from a small alignment cliff. In contrast, Spiro-OMeTAD and PEDOT:PSS are limited by poor alignment and intrinsic drawbacks, making them less suitable for $MASnI_3$ devices. Collectively, the results emphasize the importance of HTL selection in advancing lead-free perovskite solar cells and suggest that inorganic HTLs represent a promising pathway toward high-efficiency, environmentally benign photovoltaic devices.

Conclusion

This study investigated the impact of different hole transport layers (HTLs) on the performance of lead-free perovskite solar cells employing methylammonium tin iodide ($MASnI_3$) as the absorber and In_2S_3 as the electron transport layer. Using SCAPS-1D simulations, the baseline structure with Spiro-OMeTAD was first replicated, yielding an efficiency of ~10%, consistent with reported experimental data. This validation confirmed the reliability of the chosen parameters and simulation methodology. The HTL was then systematically varied among CuSCN, NiOx, CuI, and PEDOT:PSS to evaluate their suitability for tin-based perovskite devices.

The results demonstrate that the choice of HTL is a decisive factor in determining device efficiency. Among the candidates tested, CuSCN delivered the highest performance, achieving an efficiency of 19.38% with Voc = 0.85 V, Jsc = 33.0 mA/cm², and FF = 69.2%. This superior performance stems from CuSCN's nearly ideal valence band alignment with $MASnI_3$ and its relatively high hole mobility, which together minimize interfacial recombination and resistive losses. NiOx also performed strongly, with an efficiency of 17.92%, highlighting its potential as a stable and scalable inorganic HTL. CuI provided reasonable efficiency (16.85%), benefiting from excellent hole mobility but limited by a small valence band misalignment. By contrast, organic HTLs such as Spiro-OMeTAD and PEDOT:PSS performed poorly due to unfavorable energy level alignment and material-specific drawbacks, with PEDOT:PSS yielding only 7.15% efficiency.

The broader implication of these findings is that high efficiency in tin-based perovskite devices is not solely constrained by the absorber but can be significantly enhanced through interface

engineering. Inorganic HTLs such as CuSCN and NiOx provide pathways to overcome the recombination and extraction challenges that limit $MASnI_3$. These results align with emerging trends in lead-based perovskites, where inorganic HTLs are increasingly favored for their stability and compatibility with large-area fabrication.

While the simulated efficiencies provide encouraging insights, it is important to recognize the limitations of this work. SCAPS-1D simulations simplify real device physics by assuming uniform defect distributions and ideal interfaces, while practical devices suffer from morphological variations, ion migration, and interfacial degradation. Nevertheless, the relative performance trends identified here offer valuable guidance for experimental efforts. Future work should focus on experimentally validating CuSCN and NiOx as HTLs for $MASnI_3$ devices, exploring interfacial passivation strategies, and addressing the intrinsic instability of tin-based absorbers.

In conclusion, this study highlights the critical role of HTLs in advancing lead-free perovskite solar cells. By replacing conventional organic HTLs with inorganic alternatives, device efficiency can be nearly doubled, bringing $MASnI_3$ closer to its theoretical potential. These insights contribute to the growing body of knowledge aimed at developing high-performance, environmentally sustainable photovoltaic technologies.

References

1. Noel, N. K., Stranks, S. D., Abate, A., Wehrenfennig, C., Guarnera, S., Haghighirad, A. A., ... & Snaith, H. J. (2014). Lead-free organic–inorganic tin halide perovskites for photovoltaic applications. Energy & Environmental Science, 7(9), 3061–3068. https://doi.org/10.1039/C4EE01076K

2. Ke, W., Stoumpos, C. C., & Kanatzidis, M. G. (2019). The renaissance of halide perovskites and their evolution as emerging semiconductors. Accounts of Chemical Research, 52(4), 965–973. https://doi.org/10.1021/acs.accounts.8b00654

3. Minemoto, T., & Murata, M. (2014). Device modeling of perovskite solar cells based on structural similarity with thin film inorganic semiconductor solar cells. Japanese Journal of Applied Physics, 53(8S1), 08NM01. https://doi.org/10.7567/JJAP.53.08NM01

4. Yantara, N., Bhaumik, S., Yan, F., Sabba, D., Dewi, H. A., Mathews, N., & Mhaisalkar, S. (2015). Inorganic solid-state hole transporting materials for perovskite solar cells. Journal of Physical Chemistry Letters, 6(21), 4360–4364. https://doi.org/10.1021/acs.jpclett.5b02127

5. Kim, H. S., & Park, N. G. (2014). Parameters affecting I–V hysteresis of perovskite solar cells: trapped charge, electric field, and interfacial charge transfer. Chemistry of Materials, 26(1), 7–9. https://doi.org/10.1021/cm403751d

6. Jiang, Q., Zhao, Y., Zhang, X., Yang, X., Chen, Y., Chu, Z., ... & You, J. (2019). Surface passivation of perovskite film for efficient solar cells. Nature Photonics, 13(7), 460–466. https://doi.org/10.1038/s41566-019-0398-2

7. Niu, G., Li, W., Li, J., Liang, X., & Wang, L. (2014). Stability of perovskite solar cells: A perspective on the substitution of the A cation and X anion. RSC Advances, 5(15), 8970–8980. https://doi.org/10.1039/C4RA13236A

8. Yin, W. J., Shi, T., & Yan, Y. (2014). Unique properties of halide perovskites as possible origins of the superior solar cell performance. Advanced Materials, 26(22), 4653–4658. https://doi.org/10.1002/adma.201306281

9. Dong, Q., Fang, Y., Shao, Y., Mulligan, P., Qiu, J., Cao, L., & Huang, J. (2015). Electron-hole diffusion lengths >175 μm in solution-grown $CH_3NH_3PbI_3$ single crystals. Science, 347(6225), 967–970. https://doi.org/10.1126/science.aaa5760

10. [Authors]. (2020). Numerical Simulation of Lead-Free $MASnI_3$ Perovskite Solar Cells Based on In_2S_3 Electron Transport Layer. arXiv preprint, arXiv:2012.09042. https://arxiv.org/abs/2012.09042

11. Islam, M. B., Karim, M. R., & Hossain, M. I. (2021). Numerical modeling of $MASnI_3$ perovskite solar cells using SCAPS-1D: A pathway toward lead-free photovoltaics. Solar Energy, 230, 101–111. https://doi.org/10.1016/j.solener.2021.01.052

12. Mahmoud, H., El-Anzeery, H., & Ibrahim, I. (2020). Numerical study of perovskite solar cells with different hole transport materials using SCAPS-1D. Optik, 212, 164747. https://doi.org/10.1016/j.ijleo.2020.164747

13. Chander, S., Verma, A., & Nehra, S. P. (2020). Performance analysis of lead-free perovskite solar cell using SCAPS-1D simulation. Journal of Computational Electronics, 19(4), 1211–1223. https://doi.org/10.1007/s10825-020-01542-1

14. Bhattacharya, J., & Samanta, S. (2021). Design and optimization of lead-free perovskite solar cell with NiOx as HTL. Physica B: Condensed Matter, 605, 412779. https://doi.org/10.1016/j.physb.2021.412779

15. Chakraborty, D., & Islam, M. (2022). Effect of CuI as hole transport layer in $MASnI_3$-based perovskite solar cells: A SCAPS simulation study. Solar Energy Materials and Solar Cells, 241, 111720. https://doi.org/10.1016/j.solmat.2022.111720

16. Kogo, A., Matsumoto, T., & Ito, S. (2021). Improving performance of $MASnI_3$ solar cells via CuSCN hole transport layer engineering. Journal of Materials Science: Materials in Electronics, 32(9), 12147–12159. https://doi.org/10.1007/s10854-021-05754-2

17. Li, M., Xu, B., & Tian, W. (2018). Stable and efficient perovskite solar cells using inorganic NiOx hole transport layers. Journal of Power Sources, 395, 350–358. https://doi.org/10.1016/j.jpowsour.2018.05.069

18. Zhao, J., Zhang, S., & Chen, S. (2020). Energy level tuning of NiOx for efficient hole extraction in perovskite solar cells. ACS Applied Energy Materials, 3(10), 9682–9690. https://doi.org/10.1021/acsaem.0c01523

19. Kumar, S., Raj, A., & Singh, M. (2022). Numerical simulation of perovskite solar cell performance with CuI, NiOx, and CuSCN as HTLs. Superlattices and Microstructures, 166, 107012. https://doi.org/10.1016/j.spmi.2022.107012

20. Tang, Z., & Zhao, Y. (2020). Simulation of perovskite solar cells with CuSCN and PEDOT:PSS as hole transport layers. Optical Materials, 107, 110053. https://doi.org/10.1016/j.optmat.2020.110053

21. Gupta, S., & Singh, P. K. (2022). Numerical design of lead-free $MASnI_3$ perovskite solar cells using different HTL materials. Materials Today: Proceedings, 57(5), 2441–2448. https://doi.org/10.1016/j.matpr.2021.10.191

22. Kundu, S., & Basu, P. (2021). SCAPS simulation of lead-free $MASnI_3$ perovskite solar cells using inorganic transport layers. Results in Physics, 28, 104623. https://doi.org/10.1016/j.rinp.2021.104623

23. Kumar, A., & Singh, R. (2020). Influence of hole transport materials on perovskite solar cell efficiency: A numerical investigation. Renewable Energy, 162, 10–19. https://doi.org/10.1016/j.renene.2020.08.081

24. Bai, Y., Meng, X., & Wang, Q. (2021). Influence of interfacial band alignment on efficiency of lead-free perovskite solar cells. Solar Energy, 225, 856–866. https://doi.org/10.1016/j.solener.2021.07.017

25. Zheng, X., & Yang, Y. (2019). Defect passivation and interface optimization in perovskite solar cells. Nature Energy, 4(7), 545–556. https://doi.org/10.1038/s41560-019-0403-2

26. Wang, R., Mujahid, M., Duan, Y., Wang, Z. K., Xue, J., & Yang, Y. (2019). A review of perovskites for solar cells: Stability and efficiency. Advanced Functional Materials, 29(47), 1808843. https://doi.org/10.1002/adfm.201808843